

Are Pretrained Image Matchers Good Enough for SAR-Optical Satellite Registration?

Isaac Corley^{1*} Alex Stoken² Gabriele Berton²

¹Taylor Geospatial ²Independent Researcher

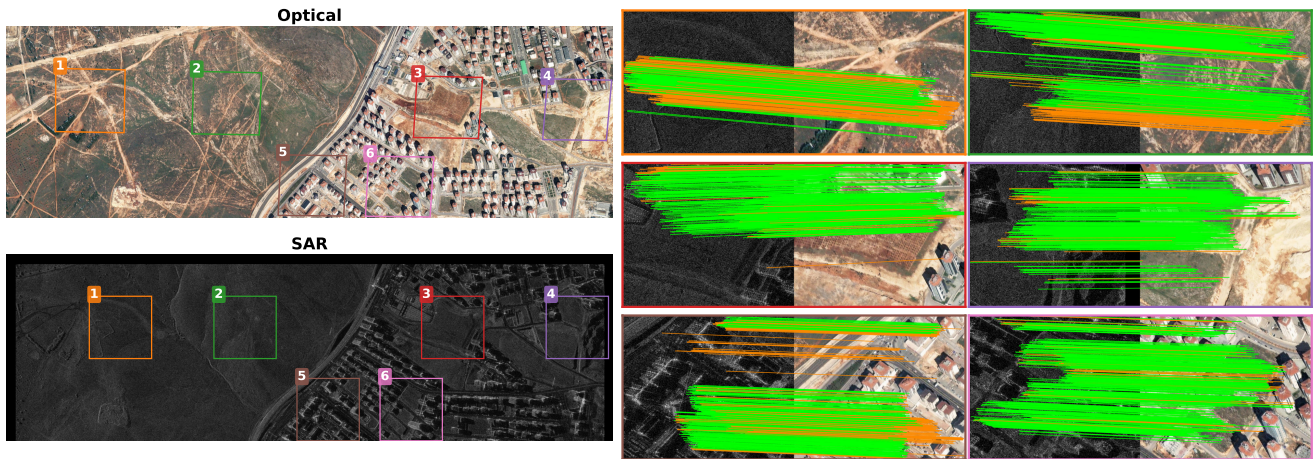


Figure 1. **Zero-shot SAR–optical registration on SpaceNet9.** Left column: full-resolution optical scene (top) and full-resolution SAR scene (bottom). Right column: tiled correspondence gallery from a zero-shot pretrained matcher—each panel shows one randomly sampled, tiepoint-projected overlapping region from the same geographic area in both modalities. Green lines denote affine-RANSAC inliers; orange lines denote outliers. Without satellite-domain fine-tuning or adaptation, a modern pretrained matcher produces dense inlier fields on SAR–optical pairs.

Abstract

Cross-modal optical–SAR (Synthetic Aperture Radar) registration is a bottleneck for disaster-response via remote sensing, yet modern image matchers are developed and benchmarked almost exclusively on natural-image domains. We evaluate twenty-four pretrained matcher families—in a zero-shot setting with no fine-tuning or domain adaptation on satellite or SAR data—on SpaceNet9 and two additional cross-modal benchmarks under a deterministic protocol with tiled large-image inference, robust geometric filtering, and tie-point-grounded metrics. Our results reveal asymmetric transfer—matchers with explicit cross-modal training do not uniformly outperform those without it. While XoFTR (trained for visible–thermal matching) and RoMa achieve the lowest reported mean error at 3.0 px on the labeled SpaceNet9 training scenes, RoMa achieves this without any cross-modal training, and MatchAnything-ELoFTR (3.4 px)—trained on synthetic cross-modal pairs—matches closely, suggesting (as a working hypothesis)

that foundation-model features (DINOv2) may contribute to modality invariance that partially substitutes for explicit cross-modal supervision. 3D-reconstruction matchers (MASt3R, DUSSt3R), which are not designed for traditional 2D image matching, are highly protocol-sensitive and remain fragile under default settings. Deployment protocol choices (geometry model, tile size, inlier gating) shift accuracy by up to 33× for a single matcher, sometimes exceeding the effect of swapping matchers entirely within the evaluated sweep—affine geometry alone reduces mean error from 12.34 to 9.74 px. These findings inform both practical deployment of existing matchers and future matcher design for cross-modal satellite registration.

1. Introduction

When a hurricane makes landfall, cloud cover often renders optical imagery unusable, leaving SAR as the primary

¹Corresponding author: isaac.corley@taylorgeospatial.org

observation modality. Registering newly acquired SAR images to pre-existing optical basemaps is necessary to produce georeferenced damage assessments within hours—a task well suited for image matching models. Yet the best pretrained image matchers are designed for indoor and urban natural-image benchmarks, not for overhead cross-modal imagery with speckle, layover, and radiometric inversion. As Robinson *et al.* [27] observe, “using satellite imagery is not simply ‘computer vision with larger images’”; Rolf *et al.* [28] make the stronger claim that satellite data constitutes a *distinct modality* whose statistical properties—overhead perspective, sensor diversity, global geographic distribution—systematically violate assumptions baked into natural-image pretraining. Do pretrained matchers survive this domain shift to overhead optical–SAR imagery, or do we need remote-sensing-specific registration methods?

Why is cross-modal satellite registration hard? Optical and SAR sensors observe the same scene through fundamentally different physics. Optical sensors record reflected sunlight, producing texture-rich imagery with familiar visual structure. SAR sensors emit and receive microwave pulses, producing imagery dominated by speckle noise, geometric layover from side-looking acquisition, and contrast inversion relative to optical data [9]. These effects create an appearance gap far larger than typical natural-image domain shifts such as day–night or indoor–outdoor variation. Classical handcrafted feature descriptors (SIFT [18], phase congruency) produce too few reliable correspondences under this gap [41]. Modern deep matchers achieve strong results on ScanNet, MegaDepth, and similar benchmarks, and recent cross-modal methods—XoFTR for visible–thermal [36], MatchAnything for multi-domain registration [10]—show that modality-aware training can improve transfer. Yet no systematic comparison across the broader matcher ecosystem exists for overhead optical–SAR imagery.

Research question. The SpaceNet9 Challenge (conducted summer 2025) formalizes this evaluation with manually verified tie points across full-resolution optical–SAR scene pairs [9, 29, 35]. Figure 1 previews the operating regime: tiled correspondence estimation on large satellite scenes where the optical–SAR modality gap challenges every stage of the matching pipeline. A common assumption is that stronger general-purpose matchers transfer broadly. Our results show this assumption fails for overhead optical–SAR imagery: correspondence quality does depend on the matcher architecture, *but also* on geometric post-processing and the registration protocol itself—tile size, overlap, inlier gating—which can shift accuracy by up to 33× for a given single matcher, sometimes exceeding the effect of swapping matchers entirely within the evaluated sweep.

We evaluate twenty-four pretrained matcher families under a fixed, zero-shot geometric protocol (with per-matcher normalization selected on the same three SpaceNet9 training scenes used for reporting) on SpaceNet9 and two additional cross-modal benchmarks (SRIF [16], SARptical [11]). Rather than proposing a new trained model, we provide controlled evidence of out-of-domain performance and isolate where pretrained matchers succeed, where they fail, and why.

Contributions.

- A reproducible zero-shot evaluation protocol for large-image cross-modal registration with tiled inference, robust geometric filtering, and tie-point-grounded metrics (§3).
- A controlled benchmark of twenty-four pretrained matchers revealing asymmetric transfer: under a fixed geometric protocol with per-matcher normalization selected on the labeled training scenes, XoFTR and RoMa achieve the lowest reported mean error (3.0 px) on SpaceNet9, with MatchAnything-ELoFTR (3.4 px) a close third, while MAST3R/DUST3R are substantially more protocol-sensitive and less stable under default settings (§5).
- Ablations across 16 protocol configurations (64 total runs) on SpaceNet9 showing that protocol parameters (geometry model, tiling, inlier gating) dominate matcher choice as the primary accuracy lever, with findings cross-validated on two additional datasets (§5).

We operationalize our titular question of “good enough” as achieving practical baseline accuracy—sub-8 px mean tie-point error on SpaceNet9 under a zero-shot protocol—with rank ordering that is qualitatively consistent across cross-modal benchmarks.

2. Related Work

Cross-modal registration. The SpaceNet9 challenge paper frames optical–SAR registration as a difficult pre-processing problem driven by radiometric and geometric modality differences, including side-looking SAR distortions and weak appearance consistency [9]. Classical handcrafted pipelines (SIFT [18], phase congruency) are often insufficient under these conditions [41], motivating deep feature-matching and learned correspondence methods for SAR–optical pairs [11, 12, 42].

Cross-modal matchers and transfer. Recent work directly targets cross-modal matching through modality-aware training. XoFTR extends LoFTR with masked image modeling pre-training and pseudo-thermal augmentation for visible–thermal matching [36], achieving 22% AUC@5° on its METU-VisTIR benchmark—an order of magnitude above LoFTR’s 2.6%. However, XoFTR eval-

uates only on ground-level visible–thermal pairs; whether this cross-modal design transfers to the harder overhead optical–SAR domain with speckle, layover, and orthorectification artifacts has not been tested. MatchAnything [10] proposes a large-scale cross-modality pre-training framework using synthetic cross-modal pairs and diverse training resources (multi-view images, video sequences, image warping). Applied to RoMa and ELoFTR base models, their framework improves SR@10 by 78.5% and 207.5% respectively on a visible–SAR satellite dataset—the closest prior evidence that cross-modal pre-training can help overhead SAR registration. However, MatchAnything evaluates only its own retrained models; no comparison across the broader matcher ecosystem exists. RoMa [7] takes an orthogonal approach: frozen DINOv2 features combined with regression-by-classification matching yield robustness to extreme appearance changes on natural image benchmarks (36% mean Average Accuracy (mAA) improvement on WxBS), but the method is evaluated exclusively on single-modality perspective imagery. MIN-IMA [13] distills modality-invariant features via multimodal pre-training across eight registration tasks, though again without overhead SAR evaluation. Few of these methods, with the exception of MatchAnything, evaluate on overhead optical–SAR imagery—the vast majority of image matching benchmarks use ground-level perspective datasets (ScanNet, MegaDepth, HPatches), leaving overhead cross-modal transfer largely unstudied. This zero-shot transfer gap extends across satellite perception tasks: Rege Cambrin *et al.* [25] show that depth foundation models require domain-specific adaptation to reliably estimate tree canopy height from satellite imagery, reinforcing that satellite data resists natural-image pretraining assumptions [28]. We address this gap by evaluating twenty-four pretrained matchers *without domain-specific fine-tuning or adaptation*, testing whether architectural priors and natural-image pre-training alone are sufficient for cross-modal transfer to overhead optical–SAR imagery.

SpaceNet9 winning solutions. Top solutions share several patterns: (i) patch-wise or tiled matching with overlap and multi-scale resizing [14, 24, 34]; (ii) local matches combined with RANSAC and affine or homography estimation, sometimes with a second refinement stage [14, 38]; (iii) modality-aware preprocessing—grayscale conversion, SAR log-compression, CLAHE (Contrast Limited Adaptive Histogram Equalization), black-border handling, building-keypoint suppression [3, 22, 34]; and (iv) robustness-oriented design over end-to-end training, given limited labeled scenes [14, 20, 24]. Our work isolates which of these protocol factors matter most by sweeping them under controlled experimental conditions.

Dataset	Modalities	Supervision	Resolution	Coverage
SpaceNet9 [9]	Optical–SAR	Tie points	~0.5 m	3 scenes
SRIF [16]	Opt–SAR/Opt–IR	Affine GT (2×3)	Varies	600 pairs
SARptical [11]	SAR–Optical patches	Binary match/no-match	~1 m	40 queries

Table 1. **Dataset summary.** Geometry-labeled sets (SpaceNet9, SRIF) support transform-grounded evaluation; the pair-only set (SARptical) supports matchability and retrieval metrics.

Multimodal benchmarks. SRIF provides affine-labeled benchmarks across optical–SAR, optical–optical, and optical–infrared pairs [16]. The concurrent SOMA-1M preprint identifies MapGlue as a strong matcher for SAR–optical registration [40], but its data and model artifacts are not yet publicly available in a form compatible with our evaluation stack, so we treat those results as related but not directly reproducible evidence.

3. Method

3.1. Task and Data

Datasets We evaluate cross-modal registration on *SpaceNet 9 train*, where three optical–SAR scene pairs include manual tie-point supervision: Scene 02_01 (151 tie points, mixed urban/suburban), Scene 02_02 (104 tie points, suburban/agricultural), and Scene 03_01 (161 tie points, dense urban). Public test data is reserved for external challenge submission scoring and is not used for local metric reporting [32].

To broaden cross-dataset coverage, we include two additional datasets. **SRIF** [16] contributes 600 valid labeled pairs (200 per modality split: optical–SAR, optical–optical, optical–infrared), each with an affine label stored as a 2×3 transform. **SARptical** [11] contributes 40 SAR query patches matched against optical candidate pools (525 total pairs per configuration) for retrieval evaluation. For each query, we run the matcher against all candidates, fit an affine model via RANSAC (threshold 3.0 px), and rank candidates by descending RANSAC inlier count; retrieval metrics (AUROC, AUPRC, Recall@ K) are computed from this ranking. Table 1 summarizes all datasets and their available supervision.

Models We evaluate only pretrained models: we apply no model weight updates (fine-tuning or domain adaptation) on satellite data. Each tested model has a different training-data mixture (some include multimodal sources), but as in typical matcher deployment settings we treat each released checkpoint as a fixed artifact and measure zero-shot transfer on this cross-modal task.

3.2. Zero-Shot Matching Protocol

Our evaluation protocol processes each optical–SAR pair through four stages:

1. Preprocessing. Each image is optionally normalized

(identity, percentile clipping to [2, 98], z-score, or Contrast-Limited Adaptive Histogram Equalization (CLAHE) with clip limit 2.0) and resized so the long side does not exceed a maximum dimension (default: 2048 px; sweep values: 1024 and 1536 px).

2. Tiled correspondence extraction. For large scenes (SpaceNet9), both images are divided into overlapping tiles (default: 768 px tiles, 256 px overlap; ablations sweep 512/128 vs. 768/256 and max resize 1024 vs. 1536). Each tile pair is fed to the matcher; tile coordinates are re-projected to the full-image frame before aggregation. Tiled inference is motivated by SpaceNet9 winning solutions that independently converged on similar strategies [14, 24]. SRIF and SARptical pairs are small enough to be processed as single images without tiling.

3. Geometric filtering. Aggregated correspondences (or single-image correspondences for SRIF/SARptical) are filtered by Random Sample Consensus (RANSAC) [8] with either an affine (2×3) or homography (3×3) model. We use OpenCV’s `estimateAffine2D` or `findHomography` with a reprojection threshold of 10 px (default). Pairs producing fewer inliers than a minimum count (default: 6; ablated at 4 vs. 6 vs. 8) are marked as failures; for tiled scenes the remaining tiles still contribute.

4. Displacement prediction. The estimated transform is applied to ground-truth tie-point coordinates (SpaceNet9) or to corner coordinates (SRIF) to produce predicted displacements, which are compared against ground truth for metric computation. We adopt fixed random seeds across all runs. All experiments were run on a single NVIDIA RTX 3090.

3.3. Metrics

On SpaceNet9 we report: (i) **mean tie-point error** (pixels), measuring displacement between predicted and ground-truth tie points; (ii) **Success@ τ** for $\tau \in \{5, 10\}$ px, the fraction of tie points with error below τ ; and (iii) **failure rate**, the fraction of pairs producing no valid geometric output (due to insufficient correspondences, unstable geometry, or degenerate transforms). Per-pair wall-clock runtime is summarized in §5.5. For SRIF, we apply the estimated transform to the four image corners and report **mean corner re-projection error** under the dataset-provided affine ground truth; success metrics use the same thresholds. For SARptical, where pair-level supervision is available without geometric labels, we report AUROC, AUPRC, and Recall@ K .

3.4. Matcher Families

We benchmark twenty-four matcher families spanning three architectural paradigms, all accessed through `vismatch` [1, 2]: *Detector-based*: XFeat and XFeat* [23] (lightweight detector, sparse and semi-dense variants),

ALIKED [43]–LightGlue [17], DeDoDe [6]–LightGlue, SuperPoint [4]–LightGlue, and DISK [37]–LightGlue (keypoint detectors with learned graph matching), GIM [30]–LightGlue and GIM-DKM (generalist image matchers), and SIFT [18]–LightGlue. *Detector-free dense*: LoFTR [33] (coarse-to-fine transformer), XoFTR [36] (cross-modal LoFTR variant), RoMa, RoMaV2, and Tiny-RoMa [7] (dense warp regression with DINOv2/3 [21, 31] backbone), MINIMA-RoMa and MINIMA-RoMa-Tiny [13] (multimodal-pretrained RoMa variants), MINIMA-XoFTR [13, 36] (multimodal-pretrained XoFTR), and MatchAnything-ELoFTR [10] (EfficientLoFTR pretrained on large-scale cross-modal data). *3D-reconstruction-derived*: MAST3R [15] and DUST3R [39], stereo reconstruction networks repurposed for 2D matching. The two are used in distinct ways. MAST3R is used as a *dense feature matcher*: we extract the per-pixel descriptors produced by its matching head and run fast reciprocal nearest-neighbor search in descriptor space to obtain 2D correspondences. DUST3R is used as a *point-cloud matcher*: its per-pixel pointmaps are globally aligned, confidence-masked, and matched by reciprocal nearest neighbors in 3D, with the corresponding 2D pixel indices returned as correspondences. Neither path uses direct 2D-coordinate regression; this distinction matters because the two failure modes (descriptor ambiguity under speckle for MAST3R vs. degenerate pointmaps under near-planar overhead geometry for DUST3R) are qualitatively different. We also include two ensembles (RoMa+LoFTR, RoMa+Tiny-RoMa) that aggregate correspondences from both matchers before geometric filtering. We additionally include classical baselines (SIFT-NN [18], HardNet [19]–LightGlue [17]) for SARptical retrieval evaluation via Kornia [26]; these serve as lower-bound references with well-understood cross-domain generalization behavior, allowing us to assess whether learned matchers offer meaningful gains over handcrafted representations on the SAR retrieval task.

4. Experiments

We run four experiment tracks: (1) broad matcher sweeps on SpaceNet9 under deterministic settings; (2) matching protocol ablations (geometry model, tiling parameters, inlier gating); (3) geometry-labeled cross-dataset evaluation on SRIF; and (4) pair-level cross-dataset ranking on SARptical. All experiments use fixed pair manifests, fixed random seeds, and identical geometric post-processing per protocol setting. Runtime is end-to-end per-pair wall-clock on a single RTX 3090, so speed ranks are comparable within this benchmark.

Variance and reproducibility. All protocols are deterministic (fixed seeds, fixed manifests); results are phrased diag-

Matcher	Norm	MeanErr↓	S@5↑	S@10↑	Fail↓
<i>Dense warp (DINOv2/3 backbone)</i>					
RoMa+Tiny-RoMa [7]	Percentile	3.6	66.6	83.8	0.00
RoMaV2 [7]	Z-Score	3.6	69.2	90.2	0.00
RoMa+LoFTR [7, 33]	Percentile	3.3	75.9	90.1	0.00
RoMa [7]	Z-Score	3.0	78.9	94.2	0.00
<i>Cross-modal / multimodal-pretrained</i>					
MINIMA-XoFTR [13, 36]	Percentile	3.8	64.6	77.3	0.00
MINIMA-RoMa [7, 13]	Percentile	3.4	66.6	79.6	0.00
MA-ELoFTR [10]	Z-Score	3.4	71.2	93.3	0.00
XoFTR [36]	Percentile	3.0	78.4	90.5	0.00
<i>Detector + graph matcher (LightGlue)</i>					
DISK-LG [17, 37]	Z-Score	4.6	52.2	82.6	0.67
ALIKED-LG [17, 43]	Percentile	4.5	62.2	84.8	0.00
DeDoDe-LG [6, 17]	Percentile	4.5	58.8	85.5	0.00
SuperPoint-LG [4, 17]	Z-Score	4.4	65.4	77.6	0.00
GIM-DKM [30]	Z-Score	4.1	57.6	85.6	0.00
<i>Detector-free dense</i>					
LoFTR [33]	Identity	5.1	54.4	81.0	0.00
<i>3D-reconstruction-derived</i>					
MASt3R [15]	Identity	4.5	60.9	80.9	0.00

Table 2. **SpaceNet9: Top-15 matchers (best norm per matcher)**. All 24 matchers evaluated under a single protocol: tiled inference (512 px tiles, 256 px overlap), affine geometry, 1024 px max side, RANSAC threshold 3.0 px, min 4 inliers. Each row shows the best normalization for that matcher. MeanErr in pixels; S@k in %; Fail in [0,1].

nostically rather than with statistical significance given only three labeled SpaceNet9 scenes. We cross-validate trends on SRIF (600 pairs) and SARptical (40 queries)—checking whether the same matcher families remain competitive under different datasets and metrics, not whether absolute scores are directly comparable. All manifests, seeds, and protocol parameters are specified in released configuration files. Code is made available at <https://github.com/isaac-corley/rsim>.

Matcher	Norm	MeanErr (px)↓	S@5↑	S@10↑	Fail↓
SuperPoint-LightGlue [17]	CLAHE	67.0	31.3	39.0	0.64
RoMa [7]	CLAHE	64.9	36.0	40.4	0.00
RoMa+LoFTR [7]	CLAHE	64.6	36.1	40.6	0.00
RoMa+Tiny-RoMa [7]	CLAHE	63.9	35.3	40.0	0.00
LoFTR [33]	CLAHE	63.3	29.7	39.4	0.65
LoFTR [33]	Z-Score	63.1	30.6	41.7	0.64
LoFTR [33]	Identity	59.3	31.9	42.3	0.66
MINIMA-RoMa [13]	Identity	48.2	42.0	45.8	0.00
MINIMA-RoMa [13]	CLAHE	47.7	40.4	44.7	0.00
MINIMA-RoMa [13]	Z-Score	47.0	41.7	45.7	0.00

Table 3. **SRIF: Normalization ablation (600 pairs)**. Top matchers from SpaceNet9 evaluated on SRIF across all three normalizations, showing sensitivity to preprocessing choice.

5. Results and Analysis

5.1. SpaceNet9 Results

Table 2 ranks the top 15 matchers on SpaceNet 9 under a fixed geometric protocol (affine geometry, 512 px

tiles, 256 px overlap, 1024 px max side, RANSAC threshold 3.0 px, ≥ 4 inliers). Each row reports the best normalization for that matcher, selected on the same three labeled training scenes used for reporting; all other protocol variables are held constant, enabling direct cross-matcher comparison. Configurations with persistent full failure are excluded from the ranking. These results should be interpreted as exploratory deployment diagnostics on the labeled training scenes rather than generalization estimates; we cross-validate ordering stability on SRIF and SARptical below.

Matcher	Norm	AUROC↑	AUPRC↑	R@1↑	R@5↑
Tiny-RoMa [7]	CLAHE	0.52	0.10	7.5	35.0
SuperPoint-LightGlue [17]	Z-Score	0.53	0.09	67.5	100.0
DISK-LightGlue [17]	Identity	0.53	0.09	70.0	97.5
LoFTR [33]	Identity	0.54	0.10	10.0	50.0
HardNet-LightGlue [19]	Identity	0.54	0.11	25.0	50.0
DUST3R [39]	CLAHE	0.55	0.10	92.5	100.0
SIFT-NN [18]	Identity	0.55	0.11	92.5	100.0
XoFTR [36]	Percentile	0.55	0.09	2.5	57.5
MA-ELoFTR [10]	Z-Score	0.56	0.11	97.5	100.0
MINIMA-RoMa [13]	Z-Score	0.57	0.11	12.5	52.5

Table 4. **SARptical: Top-10 configurations by AUROC**. Each configuration uses 40 SAR queries over 525 candidate pairs; the AUROC/AUPRC measure pair-level ranking quality over the full candidate pool, while Recall@K measures shortlist hit rate; these metrics can diverge.

5.2. Protocol Sweep

Key finding (across the evaluated ablations): protocol sensitivity can exceed matcher differences. *Deployment protocol choices affect accuracy substantially—and can exceed matcher-selection effects*—across the configurations we evaluated. Figure 2 makes this concrete: aggregating the threshold, keypoint-budget, and inlier-gating ablations across seven matchers, intra-matcher error variance across protocol configurations is often comparable to or larger than inter-matcher differences, suggesting that protocol tuning is at least as important as matcher selection on SpaceNet9. Even with XFeat, whose sparser keypoint set makes it more sensitive to matcher-level factors (e.g., requiring permissive RANSAC thresholds $t \geq 5$ px to reach competitive inlier counts)—protocol tuning yields a $>2\times$ error reduction.

We sweep 16 protocol configurations—2 geometry models (affine, homography) \times 2 max resize values (1024, 1536 px) \times 2 tile overlaps (128, 256 px) \times 2 minimum inlier counts (4, 8)—across 2 matchers (LoFTR, XFeat) and 2 normalizations (identity, percentile), yielding 64 total runs on all labeled SpaceNet9 train pairs (three scenes). Tile size is fixed at 512 px and the RANSAC reprojection threshold at 3.0 px throughout. Keypoint budget is fixed at 4096 for all sweep runs; its effect is ablated separately in §5.3.

Two trends are consistent: (1) affine geometry outperforms homography (9.74 vs. 12.34 px mean error; 0.707 vs. 0.658 Success@10). This is expected for orthorectified

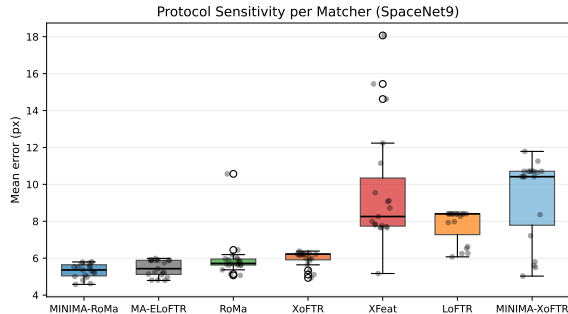


Figure 2. **Protocol sensitivity per matcher (SpaceNet9)**. Y-axis: mean error (px, \downarrow better). Each data point is one result from the threshold-robustness, keypoint-budget, or inlier-gating ablations, aggregated across seven matchers (MA-ELoFTR, MINIMA-RoMa, RoMa, XoFTR, LoFTR, MINIMA-XoFTR, XFeat; 133 total runs). *Intra*-matcher variance often matches or exceeds *inter*-matcher differences, confirming that protocol choices are a first-order deployment factor in the evaluated ablations.

satellite imagery: orthorectification removes perspective distortion, making the true sensor-to-sensor transform approximately affine (translation, rotation, scale, and shear). The additional perspective degrees of freedom in a homography (3×3 , 8 DoF) therefore absorb noise rather than signal, degrading accuracy relative to the 6-parameter affine model. (2) LoFTR with percentile normalization under affine geometry yields the best configuration (7.2 px mean error, 0.802 Success@10, 0% failure). Given the only three-scene label coverage, we treat these as interesting anecdotal comparisons and do not claim quantitative significance.

Figure 3a visualizes the affine vs. homography gap. Figure 3b shows the joint effect of tile size and overlap on accuracy for RoMa, LoFTR, and XFeat under a fixed protocol: too-small tiles with low overlap are unstable while moderate overlap improves robustness. Per-normalization sensitivity is captured in the SRIF heatmap (Figure 6).

5.3. Extended Transfer Ablations

We run threshold and inlier-gating ablations on seven matchers (MA-ELoFTR, MINIMA-RoMa, RoMa, XoFTR, LoFTR, MINIMA-XoFTR, XFeat): *threshold robustness* sweeps $t \in \{0.5, 1, 2, 3, 5, 8, 10, 15, 20\}$ px and *inlier-gating sensitivity* sweeps minimum inlier count $\in \{2, 4, 6, 8, 10\}$. The best performing configuration is MA-ELoFTR with threshold $t=15$ px achieving $S@10=0.948$ and 4.8 px mean error; MINIMA-RoMa follows at $S@10=0.901$. Inlier-gating is stable across all tested settings.

The RANSAC threshold sweep reveals non-monotonic behavior. Across matcher families, tighter thresholds improve geometric precision for strong dense matchers, while weaker or sparser matchers often require more permissive thresholds to recover enough inliers. This heterogeneity

is consistent with Edstedt’s finding that fixed RANSAC thresholds are suboptimal across domains [5]. Inlier-gating ablations show comparatively stable behavior once tiled affine fitting is active, indicating that correspondence quality and threshold selection dominate over minimum inlier count in this regime.

SARptical expanded evaluation. We evaluate all SpaceNet9-selected matchers plus (SIFT, DISK, HardNet-LightGlue) on 40 SAR queries with 525 candidate pairs per configuration. Table 4 summarizes results.

MINIMA-RoMa leads pair-ranking quality under this protocol (AUROC range across all configurations: 0.52–0.57), with narrow margins suggesting some cross-dataset robustness; among classical baselines, SIFT-NN is competitive but trails MINIMA-RoMa, while HardNet-LightGlue ranks near chance—its descriptor space does not generalize to SAR imagery. Top-10 configurations by AUROC are in Table 4; full rankings for all 24 matchers appear in the appendix.

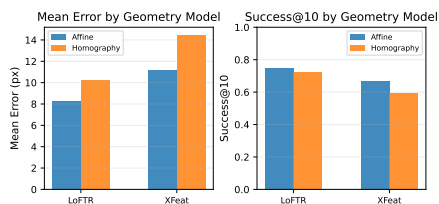
Retrieval. Recall@ K rises sharply with shortlist depth, reaching 1.0 by $K=10$, yet high Recall@ K does not imply strong global ranking (AUROC/AUPRC)—top-1 ranking remains hard under SAR–optical shift.

Across all ablations, two factors dominate accuracy in our sweeps: (i) the RANSAC reprojection threshold and (ii) the keypoint budget; retrieval shortlist depth matters for SARptical ranking, while minimum inlier count is comparatively insensitive once tiled affine fitting is active. Improving geometric verification (e.g., threshold-robust RANSAC) and multi-stage retrieval pipelines (e.g., coarse candidate selection followed by spatial verification re-ranking) will likely yield larger gains than switching matchers.

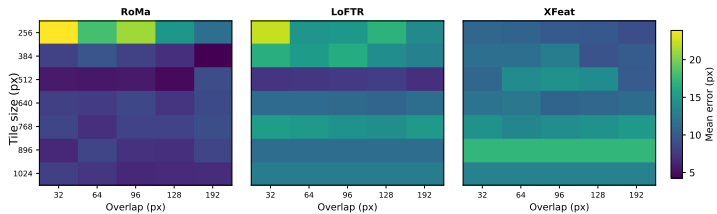
5.4. Cross-Dataset Transfer (SRIF)

To test whether SpaceNet9 matcher rankings generalize to other datasets and modality pairs—complementing the SARptical retrieval evidence above—we evaluate on SRIF (affine supervision, 600 pairs) using the same deterministic protocol family. Because SpaceNet9, SRIF, and SARptical use different primary metrics (mean tie-point error, mean corner reprojection error, and AUROC respectively), we compare relative rank ordering rather than absolute scores across datasets. When comparing SRIF results, we report both lowest mean corner reprojection error and best zero-failure trade-off, since several methods reduce error at the cost of substantial failure rates. Table 3 reports rankings over the SpaceNet9-selected matcher pool.

MA-ELoFTR achieves the lowest overall mean corner reprojection error on SRIF (45.6 px, best observed under this protocol), though at a higher failure rate (0.46). Among zero-failure methods on SRIF, MINIMA-RoMa (47.0 px, 0% failure) shows the best accuracy–reliability



(a) **Geometry-model comparison on SpaceNet9.** Affine consistently improves both mean error (\downarrow) and Success@10 (\uparrow) over homography under the evaluated sweep configurations. Orthorectification makes the true transform approximately affine, so homography’s extra DoF absorbs noise rather than signal.



(b) **Tile size vs. overlap heatmaps (RoMa/LoFTR/XFeat).** Mean error (px) under a fixed affine tiled protocol. Generally, the tile size is more influential than overlap, with results favoring tile sizes near each matcher’s training resolution.

Figure 3. **Core protocol effects on SpaceNet9.** Geometry choice and tiling interact strongly with matcher performance.

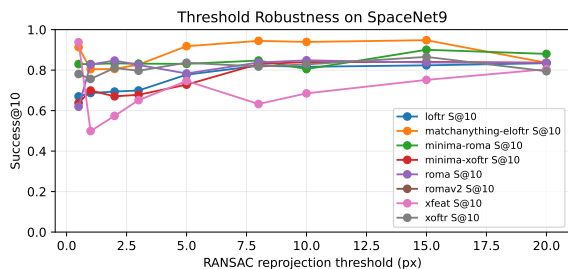


Figure 4. **RANSAC threshold robustness.** Success@10 (\uparrow better) as a function of reprojection threshold (px) for seven matchers under fixed tiled affine settings. MA-ELoFTR and MINIMA-RoMa maintain $>90\%$ success at permissive thresholds; XoFTR and RoMa follow closely. Sparser or less robust matchers (LoFTR, XFeat) are more threshold-sensitive—confirming threshold selection as a first-order deployment concern.

trade-off. This pattern is consistent with improved cross-dataset robustness for MINIMA-RoMa, especially among zero-failure methods, though the datasets and primary metrics differ. Combined with the SARptical results above, MINIMA-RoMa shows the strongest zero-failure cross-dataset consistency among the evaluated methods, even though the SpaceNet9 top rank is shared by RoMa/XoFTR. On SRIF’s easier splits (e.g., optical–optical), sparse detectors perform well because appearance differences are small; on harder modality gaps (optical–SAR, optical–infrared), detector-free dense matchers hold the advantage. Figure 6 visualizes the normalization \times matcher interaction on SRIF: MINIMA-RoMa with Z-Score normalization achieves the lowest error, but the column-wise spread indicates that normalization sensitivity varies substantially across architectures.

5.5. Discussion

Why do some matchers transfer and others fail?

XoFTR’s strong performance (lowest reported mean error on SpaceNet9, tied with RoMa) is consistent with its design: masked image modeling pre-training and pseudo-

thermal augmentation explicitly target cross-modal invariance [36], so successful transfer to optical–SAR—another cross-modal setting—is expected, even though XoFTR was trained only on visible–thermal ground-level imagery. More surprising is the competitive performance of RoMa, which has *no cross-modal training at all*. RoMa [7] is trained exclusively on single-modality perspective imagery (MegaDepth), yet achieves mean error within 1 px of XoFTR on SpaceNet9. MINIMA-RoMa [13], which does include multimodal pre-training across eight registration tasks, also ranks near the top—but the fact that RoMa alone nearly matches XoFTR without any cross-modal data suggests that architectural choices—dense warp regression over frozen DINOv2 [21] features—can yield partial modality invariance as an emergent property of foundation model pre-training on diverse internet imagery. DINOv2 is not explicitly trained for modality invariance; its web-scale pretraining may capture cross-modal correlations sufficient for partial SAR transfer. This is a plausible explanation, not a causal claim. Practitioners can achieve strong optical–SAR registration with off-the-shelf matchers; backbone diversity (via foundation model pretraining) may complement explicit cross-modal supervision rather than replace it. MAST3R and DUST3R, designed for 3D pointmap regression rather than 2D matching, assume perspective geometry and scene depth variation—both violated by orthorectified satellite imagery. As described in §3, MAST3R is repurposed as a dense feature matcher via its descriptor head and DUST3R as a point-cloud matcher via reciprocal 3D-NN over its pointmaps, so their failure modes are not identical. DUST3R’s pointmap path is most directly hurt by near-planar overhead geometry: its 3D regression heads produce geometrically inconsistent pointmaps when depth variation is minimal, yielding degenerate reciprocal matches that cause RANSAC to fail. MAST3R’s descriptor path appears to fail more gracefully under the same geometry (consistent with its top-15 placement in Table 2), though it likely still suffers from weak descriptor discriminability

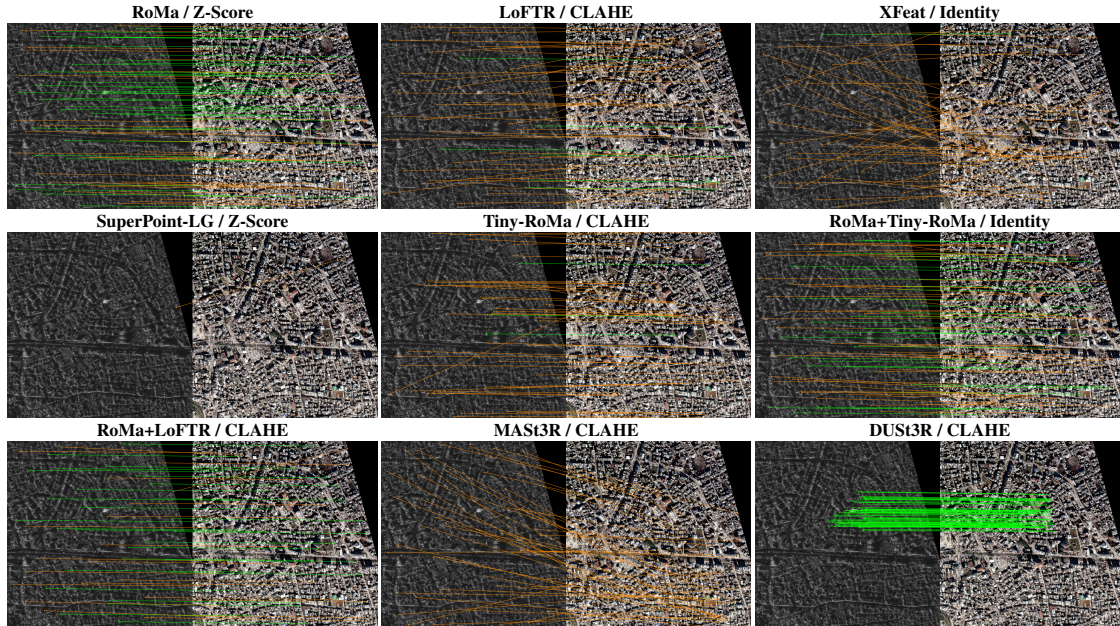


Figure 5. **SpaceNet9 qualitative correspondence gallery.** Panels show top matchers under their best zero-shot configurations; green lines denote affine-RANSAC inliers and orange lines matched outliers.

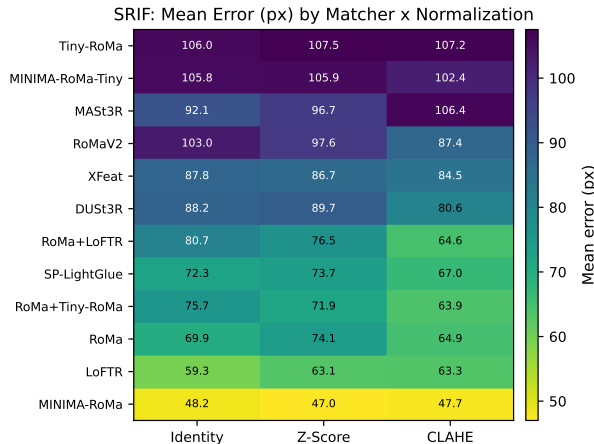


Figure 6. **Normalization × matcher heatmap (SRIF).** Cell values are mean corner reprojection error (px). Column-wise spread illustrates that normalization choice can have marked performance impacts on matchability. More spread indicates a matcher with greater sensitivity to normalization scheme. MINIMA-RoMa with Z-Score achieves the lowest error.

under speckle and radiometric inversion; we offer this as a plausible explanation rather than a causal claim. Their training data (ScanNet, CO3D) also contains no overhead or SAR views, unlike DINOv2’s web-scale pretraining. This geometric and domain mismatch explains their fragility under default settings.

Protocol vs. matcher: which matters more? As quantified in Figure 2 and discussed in §5, protocol choices can equal or exceed matcher selection effects in the eval-

uated configurations. Switching MAST3R from default to relaxed tiling yields a $33\times$ error reduction, larger than the gap between the worst and best matchers under any fixed protocol. Similarly, switching from homography to affine geometry reduces mean error by 2.6 px on average (Figure 3a)—comparable to the gap between mid-tier and top-tier matchers—and this trend holds across SRIF and SARp-tical, not just SpaceNet9.

Practical deployment guidance. Our ablations point to a concrete protocol baseline for optical-SAR registration: (i) affine geometry over homography; (ii) 768×768 tiles with ≥ 128 px overlap; (iii) percentile or CLAHE normalization; (iv) RANSAC threshold ≤ 10 px; and (v) MINIMA-RoMa or RoMa as the default matcher for zero-shot deployment under the evaluated protocols. Tile overlap and minimum inlier count are comparatively insensitive and can be fixed at reasonable defaults without further tuning. This baseline achieves <8 px mean error on SpaceNet9 and 47.0 px on SRIF without any domain-specific training.

Computational cost. Table 5 reports per-pair end-to-end wall-clock on a single NVIDIA RTX 3090 under the Table 2 protocol. Runtime spans more than an order of magnitude, from 0.3 s (XFeat-Star) to 11.5 s (OmniGlue), and the accuracy-cost trade is approximately monotonic: higher-accuracy RoMa variants and their ensembles sit at the slow end, and the cheapest detectors pay for their speed in accuracy. The clear Pareto outlier is XoFTR, which sits in the top accuracy tier on Table 2 at ≈ 0.4 s per pair—roughly an order of magnitude faster than the RoMa family—and is the

Matcher	T(s)	Matcher	T(s)
XFeat-Star	0.3	DeDoDe-LG	3.8
XFeat	0.3	RoMaV2	4.1
Tiny-RoMa	0.3	MA-ELoFTR	4.7
MINIMA-RoMa-Tiny	0.4	DUST3R	4.9
XoFTR	0.4	RoMa	5.0
SIFT-NN	0.4	MINIMA-XoFTR	5.3
SuperPoint-LG	0.4	MINIMA-RoMa	5.5
ALIKED-LG	0.5	GIM-DKM	5.5
DISK-LG	0.9	LoFTR	5.6
GIM-LG	0.9	RoMa+LoFTR	6.7
SIFT-LG	1.4	RoMa+Tiny-RoMa	6.8
MASt3R	2.5	OmniGlue	11.5

Table 5. **Per-pair runtime on SpaceNet9 (RTX 3090).** End-to-end wall-clock per pair (tile extraction, matcher forward pass, and RANSAC fit) under the Table 2 protocol (1024 px max side, 512×512 tiles with 256 px overlap, ~4 tiles per pair), averaged over all labeled SpaceNet9 pairs. Sorted by time within each column; matchers span more than an order of magnitude. Preprocessing and I/O are excluded as they are essentially constant across matchers.

strongest default when per-pair latency matters at scale.

6. Limitations

Scene and annotation coverage. SpaceNet9 train provides only three labeled scenes with residual annotation and geolocation noise; scene-level statistical power is limited despite sweeping 64 protocol configurations per matcher. Results should be treated as diagnostic evidence at the pair and tile level, not statistically independent scene samples.

Matcher coverage and adaptation scope. We evaluate twenty-four families available through `vismatch` at the time of experimentation; MapGlue [40] and other recently released matchers are not yet integrated. We evaluate only pretrained matchers without adaptation—lightweight fine-tuning (e.g., adapter modules or modality-specific pretraining as in XoFTR [36]) may close the gap for fragile matchers like MASt3R and DUST3R.

7. Conclusion

We present a systematic zero-shot evaluation of twenty-four pretrained matchers on optical–SAR registration across SpaceNet9, SRIF, and SARptical. XoFTR and RoMa achieve the lowest reported mean tie-point error (3.0 px) on SpaceNet9, with MatchAnything-ELoFTR (3.4 px) a close third. Protocol choices shift accuracy by up to 33×, sometimes exceeding matcher-swap effects; rank ordering is qualitatively consistent across datasets, with MINIMA-RoMa showing the strongest zero-failure cross-dataset consistency among the evaluated methods.

References

[1] Gabriele Berton and contributors. `vismatch`: Wrapper of 50+ image matching models with a unified interface. <https://github.com/gmberton/vismatch>, 2026. GitHub repository, accessed 2026-02-21. 4

[2] Gabriele Berton, Gabriele Goletto, Gabriele Trivigno, Alex Stoken, Barbara Caputo, and Carlo Masone. Earthmatch: Iterative coregistration for fine-grained localization of astronaut photography. In *Proceedings of the IEEE/CVF Conference on Computer Vision and Pattern Recognition (CVPR) Workshops*, 2024. 4

[3] Giovanni Cavallin. Spacenet9 final report (4th place), 2025. Winning technical report (SpaceNet9 Challenge). 3

[4] Daniel DeTone, Tomasz Malisiewicz, and Andrew Rabinovich. SuperPoint: Self-supervised interest point detection and description. In *CVPR Workshops*, 2018. 4, 5

[5] Johan Edstedt. Less biased noise scale estimation for threshold-robust ransac. In *CVPR 2025 Workshops (IMW)*, 2025. 6

[6] Johan Edstedt, Georg Athanasiadis, Marten Bülow, and Mårten Wadenbäck. DeDoDe: Detect, don’t describe—describe, don’t detect for local feature matching. In *3DV*, 2024. 4, 5

[7] Johan Edstedt, Qiyu Sun, Georg Bökman, Mårten Wadenbäck, and Michael Felsberg. RoMa: Robust dense feature matching. In *CVPR*, 2024. 3, 4, 5, 7

[8] Martin A. Fischler and Robert C. Bolles. Random sample consensus: A paradigm for model fitting with applications to image analysis and automated cartography. *Communications of the ACM*, 24(6):381–395, 1981. 4

[9] Ronny H’ansch, Jacob Arndt, Philippe Dias, Abhishek Potnis, Dalton Lunga, Desiree Petrie, and Todd M. Bacastow. Introducing spacenet9 – cross-modal satellite imagery registration for natural disaster responses. In *IGARSS 2024 - 2024 IEEE International Geoscience and Remote Sensing Symposium*, 2024. 2, 3

[10] Xingyi He, Hao Yu, Sida Peng, Dongli Tan, Zehong Shen, Hujun Bao, and Xiaowei Zhou. MatchAnything: Universal cross-modality image matching with large-scale pre-training. *arXiv preprint arXiv:2501.07556*, 2025. 2, 3, 4, 5

[11] Lloyd H. Hughes, Michael Schmitt, Lichao Mou, Yuanyuan Wang, and Xiao Xiang Zhu. Identifying corresponding patches in SAR and optical images with a pseudo-siamese CNN. *IEEE Geoscience and Remote Sensing Letters*, 15(5): 784–788, 2018. 2, 3

[12] Lloyd Haydn Hughes, Diego Marcos, Sylvain Lobry, Devis Tuia, and Michael Schmitt. A deep learning framework for matching of SAR and optical imagery. *ISPRS Journal of Photogrammetry and Remote Sensing*, 169:166–179, 2020. 2

[13] Xingyu Jiang, Jiangwei Ma, Xinying Hu, Yao Tai, Chengjie Wang, and Jian Yang. MINIMA: Modality invariant image matching. In *NeurIPS*, 2024. 3, 4, 5, 7

[14] Motoki Kimura. Spacenet9 final report (2nd place), 2025. Winning technical report (SpaceNet9 Challenge). 3, 4

[15] Vincent Leroy, Yohann Cabon, and Jérôme Revaud. Grounding image matching in 3D with MASt3R. In *ECCV*, 2024. 4, 5

[16] Jiayuan Li, Qingwu Hu, and Yongjun Zhang. Multimodal image matching: A scale-invariant algorithm and an open

- dataset. *ISPRS Journal of Photogrammetry and Remote Sensing*, 204:77–88, 2023. 2, 3
- [17] Philipp Lindenberger, Paul-Erik Sarlin, and Marc Pollefeys. LightGlue: Local feature matching at light speed. In *ICCV*, 2023. 4, 5
- [18] David G. Lowe. Distinctive image features from scale-invariant keypoints. *International Journal of Computer Vision*, 60(2):91–110, 2004. 2, 4, 5
- [19] Anastasiya Mishchuk, Dmytro Mishkin, Filip Radenović, and Jiří Matas. Working hard to know your neighbor’s margins: Local descriptor learning loss. In *NeurIPS*, 2017. 4, 5
- [20] Andrea Nascetti. Spacenet9 final report (1st place), 2025. Winning technical report (SpaceNet9 Challenge). 3
- [21] Maxime Oquab, Timothée Darcet, Théo Moutakanni, Huy Vo, Marc Szafraniec, Vasil Khalidov, Pierre Fernandez, Daniel Haziza, Francisco Massa, Alaaeldin El-Nouby, et al. DINOv2: Learning robust visual features without supervision. *Transactions on Machine Learning Research*, 2024. 4, 7
- [22] Jesús Orozco Gómez. Spacenet9 final report (5th place), 2025. Winning technical report (SpaceNet9 Challenge). 3
- [23] Guilherme Potje, Felipe Cadar, Andre Araujo, Renato Martins, and Erickson R. Nascimento. XFeat: Accelerated features for lightweight image matching. In *CVPR*, 2024. 4
- [24] Roman Pyankov. Spacenet9 final report (3rd place), 2025. Winning technical report (SpaceNet9 Challenge). 3, 4
- [25] Daniele Rege Cambrin, Isaac Corley, and Paolo Garza. Depth any canopy: Leveraging depth foundation models for canopy height estimation. In *European Conference on Computer Vision*, pages 71–86. Springer, 2024. 3
- [26] Edgar Riba, Dmytro Mishkin, Daniel Ponsa, Ethan Rublee, and Gary Bradski. Kornia: an open source differentiable computer vision library for pytorch. In *Proceedings of the IEEE/CVF Winter Conference on Applications of Computer Vision*, pages 3674–3683, 2020. 4
- [27] Caleb Robinson, Nils Lehmann, Adam J Stewart, Burak Ekim, Heng Fang, Isaac A Corley, and Mauricio Cordeiro. Advancing earth observation through machine learning: A torchgeo tutorial. *arXiv preprint arXiv:2603.02386*, 2026. 2
- [28] Esther Rolf, Konstantin Klemmer, Caleb Robinson, and Hannah Kerner. Mission critical–satellite data is a distinct modality in machine learning. *arXiv preprint arXiv:2402.01444*, 2024. 2, 3
- [29] Kelly Schroeder. Cross-modal satellite imagery registration. <https://spacenet.ai/sn9-challenge/>, 2025. SpaceNet 9 overview page, accessed 2026-02-21. 2
- [30] Xuelun Shen, Zhipeng Yin, Xin Wang, Xuehui Chen, Zijin Chen, Xiao Bai, Jian Wang, and Hongbo Gao. GIM: Learning generalizable image matcher from internet videos. In *ICLR*, 2024. 4, 5
- [31] Oriane Siméoni, Huy V. Vo, Maximilian Seitzer, Federico Baldassarre, Maxime Oquab, Cijo Jose, Vasil Khalidov, Marc Szafraniec, Seungeun Yi, Michaël Ramamonjisoa, Francisco Massa, Daniel Haziza, Luca Wehrstedt, Jianyuan Wang, Timothée Darcet, Théo Moutakanni, Leonel Sentana, Claire Roberts, Andrea Vedaldi, Jamie Tolan, John Brandt, Camille Couprie, Julien Mairal, Hervé Jégou, Patrick Labatut, and Piotr Bojanowski. Dinov3, 2025. 4
- [32] SpaceNetChallenge. Spacenet9 challenge repository. <https://github.com/SpaceNetChallenge/SpaceNet9>, 2026. GitHub repository, accessed 2026-02-21. 3
- [33] Jiaming Sun, Zehong Shen, Yuang Wang, Hujun Bao, and Xiaowei Zhou. LoFTR: Detector-free local feature matching with transformers. In *CVPR*, 2021. 4, 5
- [34] Dongli Tan. Spacenet9 final report (top graduate), 2025. Winning technical report (SpaceNet9 Challenge). 3
- [35] Topcoder. Spacenet 9: Cross-modal satellite imagery registration. <https://www.topcoder.com/challenges/9620f66a-767e-40ac-81d5-5cc61274b186>, 2025. Challenge page, accessed 2026-02-21. 2
- [36] Önder Tuzcuoğlu, Aybora Köksal, Buğra Sofu, Sinan Kalkan, and A. Aydın Alatan. XoFTR: Cross-modal feature matching transformer. In *CVPR 2024 Workshops (IMW)*, 2024. 2, 4, 5, 7, 9
- [37] Michał Tyszkiewicz, Pascal Fua, and Vincent Lepetit. DISK: Learning local features with policy gradient. In *NeurIPS*, 2020. 4, 5
- [38] Poojan Vachharajani. Spacenet9 final report (top undergraduate), 2025. Winning technical report (SpaceNet9 Challenge). 3
- [39] Shuzhe Wang, Vincent Leroy, Yohann Cabon, Boris Chidlovskii, and Jérôme Revaud. DUST3R: Geometric 3d vision made easy. In *CVPR*, 2024. 4, 5
- [40] Peihao Wu, Yongxiang Yao, Yi Wan, Wenfei Zhang, Ruipeng Zhao, Jiayuan Li, and Yongjun Zhang. SOMA-1M: A large-scale SAR-optical multi-resolution alignment dataset for multi-task remote sensing, 2026. 3, 9
- [41] Yuming Xiang, Rongshu Tao, Feng Wang, Hongjian You, and Bing Han. Automatic registration of optical and SAR images via improved phase congruency model. *IEEE Journal of Selected Topics in Applied Earth Observations and Remote Sensing*, 13:5847–5861, 2020. 2
- [42] Han Zhang, Weiping Ni, Weidong Yan, Deliang Xiang, Junzheng Wu, Xiaoliang Yang, and Hui Bian. Registration of multimodal remote sensing image based on deep fully convolutional neural network. *IEEE Journal of Selected Topics in Applied Earth Observations and Remote Sensing*, 12(8): 3028–3042, 2019. 2
- [43] Xiaoming Zhao, Xingming Wu, Jiabi Miao, Weihai Chen, Peter C. Y. Chen, and Zhengguo Li. ALIKED: A lighter keypoint and descriptor extraction network via deformable transformation. In *IEEE Transactions on Instrumentation and Measurement*, 2023. 4, 5